ORIGINAL RESEARCH

Preparation and evaluation of tacrolimus-loaded thermosensitive solid lipid nanoparticles for improved dermal distribution

Ji-Hyun Kang[1],*
Jinmann Chon[2],*
Young-Il Kim[1]
Hyo-Jung Lee[1]
Dong-Won Oh[1]
Hong-Goo Lee[1]
Chang-Soo Han[1]
Dong-Wook Kim[3]
Chun-Woong Park[1]

[1]College of Pharmacy, Chungbuk National University, Cheongju, Republic of Korea; [2]School of Medicine, Kyung Hee University, Seoul, Republic of Korea; [3]Department of Pharmaceutical Engineering, Cheongju University, Cheongju, Republic of Korea

*These authors contributed equally to this work

Correspondence: Chun-Woong Park
College of Pharmacy, Chungbuk National University, 194-21, Osongsangmyeong 1-ro, Heungdeok-gu, Cheongju, Chungbuk 28160, Republic of Korea
Tel +82 43 261 3330
Fax +82 43 268 2732
Email cwpark@cbnu.ac.kr

Dong-Wook Kim
Department of Pharmaceutical Engineering, Cheongju University, 298, Deasung-ro, Cheongwon-gu, Cheongju, Chungbuk 28503, Republic of Korea
Tel +82 43 229 7984
Fax +82 43 229 8577
Email pharmengin@cju.ac.kr

Background: Tacrolimus (TCR), also known as FK-506, is a biopharmaceutics classification system (BCS) class II drug that is insoluble in water because of its high log P values. After dermal application, TCR remains in the stratum corneum and passes through the skin layers with difficulty.

Purpose: The objectives of this study were to develop and evaluate solid lipid nanoparticles (SLNs) with thermosensitive properties to improve penetration and retention.

Methods: We prepared TCR-loaded thermosensitive solid lipid nanoparticles (TCR-SLNs) with different types of surfactants on the shell of the particle, which conferred the advantages of enhancing skin permeation and distribution. We also characterized them from a physic point of view and performed in vitro and in vivo evaluations.

Results: The TCR contained in the prepared TCR-SLN was in an amorphous state and entrapped in the particles with a high loading efficiency. The assessment of ex vivo skin penetration using excised rat dorsal skin showed that the TCR-SLNs penetrated to a deeper layer than the reference product (0.1% Protopic®). In addition, the in vivo skin penetration test demonstrated that TCR-SLNs delivered more drug into deeper skin layers than the reference product. FT-IR images also confirmed drug distribution of TCR-SLNs into deeper layers of the skin.

Conclusion: These results revealed the potential application of thermosensitive SLNs for the delivery of difficult-to-permeate, poorly water-soluble drugs into deep skin layers.

Keywords: tacrolimus, thermosensitive, solid lipid nanoparticle, FT-IR imaging, atopic dermatitis, dermal delivery

Introduction

Tacrolimus (TCR) has shown notable therapeutic efficacy for immune-inflammatory conditions, including atopic dermatitis (AD).[1] In 1999, TCR ointment, sold under the brand name Protopic® (Astellas Pharma, Japan), was approved by the US-FDA to treat moderate to severe cases of AD. TCR is a biopharmaceutics classification system (BCS) class II drug, with low solubility and high permeability.[2] However, the physicochemical properties of TCR, namely its high molecular weight (822.95 g/mol) and strong lipophilicity (partition coefficient log P=3.96±0.83), indicate that it cannot readily pass through the skin barrier and penetrate into deeper skin layers.[3] Previous research showed that when TCR was dermally applied, most of the drug did not penetrate the skin and remained in the stratum corneum.[4] A new delivery system is therefore needed to allow greater penetration of TCR into the target areas, such as the

epidermis and dermis, which are deeper in the skin than the stratum corneum. Currently, various delivery systems for TCR, such as polymeric micelle nanocarriers,[5] solid lipid nanoparticles (SLNs),[6] and nanosized lipid carriers[7] are being actively studied. However, no reference products have yet been developed to overcome the drawback such as low solubility and strong lipophilicity.

SLNs were developed in the early 1990s as an alternative drug delivery and carrier system to liposomes, emulsions, and polymeric nanoparticles. SLNs are produced by replacing the liquid lipid (oil) of an oil/water (o/w) emulsion with a solid lipid or a blend of solid lipids, such that the lipid particle matrix is solid at both room and body temperatures.[8] SLN formulations for various application routes (parenteral, oral, transdermal, ocular, pulmonary, and rectal) have been developed and thoroughly characterized in vitro and in vivo.[9,10] The incorporation of cosmetic and pharmaceutical actives has been demonstrated to be feasible. The mean particle size of SLNs is in the submicron range, from approximately 40 to 1000 nm. SLNs combine the advantages of colloidal carriers and overcome some of their disadvantages. The SLN system offers many advantages for the target drug, such as the improved bioavailability of poorly water-soluble molecules or drugs.[11] SLNs also have advantages such as site-specific drug delivery, greater stability than liposomes, the ability to use biodegradable physiological lipids thereby decreasing the risk of acute and chronic toxicities, and the avoidance of organic solvents during production.[12–14] SLNs have previously been developed with many advantageous characteristics for dermal and topical application.[15,16] Their small size, of approximately 200 nm or less, ensures close contact with the stratum corneum and increased skin penetration of the drug. SLN formulations have been studied to determine their ability to improve the skin permeation of hydrophobic agents commonly used in cosmetics, such as coenzyme Q10,[17] tocopherol (vitamin E),[18] and retinol (vitamin A).[19] The improved transdermal uptake of active compounds loaded into SLNs also result from an increase in the contact surface area between the active pharmaceutical ingredient and the corneocytes, a more rapid or extended release, and the use of surfactants as enhancers.[20]

SLNs have been studied with classification of functional properties such as pH sensitive, thermosensitive, light responsive, and ultrasound responsive. Thermosensitive SLNs deposit or accumulate in the target sites through passive or active mechanisms, allowing efficient control of the distribution of the encapsulated active pharmaceutical ingredient (API) with a notable decrease in adverse events and drug wastage. Moreover, when SLNs reached the maximum accumulation in the target sites, sustained release of the encapsulated API occurred in response to changes in environmental factors, such as temperature. For example, many researchers have studied heat-sensitive nanoparticles that released drug only in heated lesions.[21–23] High-intensity focused ultrasound (HIFU), used in cancer treatment, has also been applied. Several studies have investigated the release of drugs from thermosensitive nanoparticles as the temperature of cancer tissues is increased by HIFU.[24–27] In addition, studies have been conducted to visualize the thermosensitive particles. Magnetic resonance imaging was used to track thermosensitive liposomes in vitro and in vivo.[28–30] Indeed, it would be most desirable if the drugs could be efficiently administered in a manner that precisely matched the physiological needs at the proper sites and at proper times.[31] In this study, as the temperature varied depending on the depth of the skin (for example, the stratum corneum contacting the outermost part of the skin is 30 °C to 31 °C and the temperature of the deep inner dermis is maintained at 36 °C to –37 °C), the use of SLNs with thermosensitive properties has great potential to be an important novel drug delivery system. The objectives of this study were to develop and evaluate SLNs with thermosensitive properties to improve skin retention, and to visualize the improved penetration through ex vivo and in vivo experiments by using FT-IR imaging.

Materials and methods
Materials

TCR was purchased from CKD Bio Corporation (Ansan, Korea). Cocoglyceride was obtained from BASF (Ludwigshafen, Germany). The reference product was 0.1% Protopic® ointment (Astellas Pharm, Tokyo, Japan). Stearic acid was purchased from Tokyo Chemical Industry Co. Ltd (Tokyo, Japan). Poloxamer 188 was supplied by Croda International (Snaith, UK), and soybean lecithin was purchased from Samchun Chemical (Pyeongtaek, Korea). Brij® 93 and Brij® 58 were purchased from Sigma Aldrich Corporation (St. Louis, USA). Methylene chloride was purchased from OCI Corporation (Seoul, Korea). High-performance liquid chromatography (HPLC) grade ethanol and acetonitrile were purchased from Honeywell Burdick & Jackson (Muskegon, USA). Water was purified by filtration in the laboratory. HPLC-

grade solvents were used for the analysis. Sprague Dawley® Rats and New Zealand white rabbits were purchased from Samtako Corporation (Osan, Korea).

Methods
Preparation of SLNs
TCR-SLNs were prepared by using a modified method of previously studied emulsification and low temperature solidification.[32] The drug-oil and lipid phases were separately prepared. The drug-oil phase and lipid phase was mixed at 5,000 rpm and 50 °C for 20 min using a homogenizer. The drug-oil-lipid phase was injected slowly into an aqueous phase at 70 °C over 15 min, and then mixed at 15,000 rpm and 70 °C for 20 min using a homogenizer. The mixture was rapidly poured into an ice-water in chiller (RW-0525G, Jeiotech®, Daejeon, Korea) at 0 °C to form the TCR-SLN emulsion. The mixture was sonicated in the chiller at 0 °C by using a probe sonicator (VP-5S, Taitec® Corporation, Koshigaya, Japan) to obtain a stable TCR-SLN suspension. The blank SLN suspension was obtained by using the same method in the absence of TCR when preparing the drug-oil-lipid phase (Table 1). The composition of each TCR-SLN is described in Table 2, and the method of preparing each phase is briefly described. The drug-oil phase was obtained by accurately weighing cocoglyceride and TCR and dissolving them in methylene chloride. Soybean lecithin and Brij® 93 were dissolved in ethanol by using a homogenizer (T-18, IKA®, Staufen, Germany) at 5,000 rpm and 50 °C for 20 min to the obtain the lipid phase. The aqueous phase comprised 2% (w/v) surfactant in distilled water.

Physicochemical characterization of TCR-SLNs
Particle size distribution and entrapment efficiency
The particle size and polydispersity index were detected by using a zeta-size analyzer (Portal ELSZ size analyzer, Otsuka® Electronics, Osaka, Japan). Measurements were performed at an angle of 90° and a temperature of 25 °C. One milliliter of TCR-SLN suspension was added to the cuvette and the particle size was measured. Each experiment was conducted three times.

The prepared TCR-SLNs (500 µL) were filtered through an Amicon® Ultrafilter 10 kDa (Merck Millipore, Burlington, USA) and centrifuged (MEGA17R, Hanil Science Medical, Daejeon, Korea) at 17,500 rpm and 4 °C for 50 min. The filtered solution was diluted 10 times with the mobile phase and TCR was quantified using HPLC. The column properties were: 5 µm, C18 100Å, 150×4.6 mm (Youngjin Biochrom Co., Ltd, Seongnam, Korea). The

Table 1 Formulations of blank-SLNs

	Excipient	SLN-B1	SLN-B2	SLN-B3	SLN-B4	Solvent
Oil phase	Cocoglyceride	0.4 g	0.4 g	0.4 g	0.4 g	Methylene chloride
Lipid phase	Lecithin Brij® 93	0.3 g 1.0 g	0.3 g 1.0 g	0.3 g 1.0 g	0.3 g 1.0 g	Ethanol
Aqueous phase	Poloxamer 188 PEG-40 stearate Brij® 58 PEG-1000	1.0 g – – –	– 1.0 g – –	– – 1.0g –	– – – 1.0 g	Distilled water

Table 2 Formulations of TCR-SLNs

	Excipient	TCR-SLN-1	TCR-SLN-2	Solvent
Drug-oil phase	Coco glyceride Tacrolimus	0.4 g 0.1 g	0.4 g 0.1 g	Methylene chloride
Lipid phase	Lecithin Brij® 93	0.3 g 1.0 g	0.3 g 1.0 g	Ethanol
Aqueous phase	Poloxamer 188 Brij® 58	1.0 g –	– 1.0 g	Distilled water

mobile phase was a mixture of acetonitrile and distilled water solution (70:30 v/v), which was filtered through a 0.2 μm membrane filter (Sartorius, Gottingen, Germany) and then degassed before use. The mobile phase was pumped at a flow rate of 1.1 mL/min. The column temperature was set at 50 °C, and the detection wavelength was set at 210 nm.

The entrapment efficiency was calculated from the following equation

$$\text{Entrapment efficiency (\%)} = \frac{C_{initial\,drug} - C_{free\,drug}}{C_{initial\,drug}} \times 100$$

Where $C_{initial\,drug}$ is the concentration of the initial TCR-SLN suspension used for the preparation of TCR-SLN and $C_{free\,drug}$ is the concentration of free TCR detected in the residual solution after centrifugation.

Differential scanning calorimetry

The thermal properties of the TCR raw material, other excipients, blank-SLNs, and prepared TCR-SLNs were analyzed by using a DSC Q2000 (TA Instruments, New Castle, USA) thermal analyzer system. Blank-SLNs and prepared TCR-SLNs were lyophilized by using a FreeZone 2.5 L Benchtop Freeze Dry System (LABCONCO®, Kansas City, USA), which removed all water to leave a dry powder. The samples were accurately weighed, loaded into an aluminum pan, and analyzed at a heating rate of 10 °C/min over a temperature range of 20 °C to 200 °C. The thermal response of the prepared sample was calculated by using TA Advantage/ Universal Analysis software (v5.2.6). The crystallinity of the prepared TCR-SLNs was determined from the enthalpy of Tm in the DSC.

X-ray diffraction

X-ray diffraction (XRD) patterns of the TCR raw material, other excipients, physical mixture, and lyophilized TCR-SLNs were analyzed by using the D8 Discover with GADDS (Bruker AXS, Karlsruhe, Germany) at a wavelength of 1.54 Å. The 2θ scans were conducted between 5° and 60°.

Fourier-transform infrared spectroscopy

Infrared spectroscopy was performed by using a Fourier transform infrared (FT-IR) spectrophotometer (4100 Jasco Tokyo, Japan). For each spectrum, 16 transient spectra were collected over the range 650–4000 cm^{-1} for the TCR, Brij® 58, Poloxamer 188, the physical mixture, and the prepared TCR-SLNs.

Transmission electron microscopy

Transmission electron microscopy (TEM) was used to visualize the morphology and structure of the prepared TCR-SLNs. First, the copper grid (TED PELLA Corporation, Redding, USA) was soaked in a drop of TCR-SLN suspension for 1 min. Subsequently, the particles on the grid were dyed with 2% (w/v) phosphotungstic acid solution for 10 s and washed twice with distilled water for 1 s. The grids were dried for approximately 30 min at temperatures of 25 °C, 37 °C, and 50 °C. The images of prepared particles were captured by using LIBRA 120 (Carl Zeiss, Oberkochen, Germany) with an accelerating voltage of 200 kV.

In vitro/ex vivo evaluation of TCR-SLNs

In vitro release test of TCR-SLNs

In vitro release studies were performed by using 12 mL Franz-diffusion cells (16 mm in diameter). The Franz-diffusion cell was regulated at 37 °C by using a water jacket and the Franz-box was maintained at 32 °C. Dialysis membrane (Spectra/Por® 2 dialysis membrane standard RC sheets, Repligen Corporation, Waltham, USA) with a molecular weight cut-off (MWCO) of 12–14 kDa and a pore size of 2.4 nm were used for the release experiments. Ethanol and pH 7.4 phosphate buffer solution (PBS) were mixed in a 3:7 (v/v) ratio and used as the receptor phase. A 500 μL aliquot of the prepared TCR-SLNs (0.1% TCR) was applied to the donor compartment and covered with Parafilm® to prevent drying. The concentration of TCR in the samples from receptor fluid was analyzed by using HPLC.

Ex vivo skin penetration test of TCR-SLNs

The ex vivo skin penetration test of TCR-SLNs was conducted by using excised rat dorsal skin samples from 8-week-old Sprague Dawley rats. The skins were hydrated with PBS and then mounted in the Franz-diffusion cell. The pH 7.4 PBS containing ethanol (30% v/v) was used as the receptor fluid. The dorsal skin was in full contact with the receptor phase. A 500 μL aliquot of the prepared TCR-SLNs (0.1% w/w TCR) and 500 mg of the reference product were applied to the donor compartment and covered with Parafilm® to prevent drying. Ex vivo skin penetration was examined over a 24 h period. The stratum corneum was separated by using adhesive tape (3M Scotch®) and the dermis/epidermis was cut into six pieces.[33] Each piece was placed in a 15 mL conical tube with 5 mL of mobile phase and sonicated to extract the TCR. Subsequently, the solution was filtered through a

0.45 μm pore syringe filter (Whatman^{TM} 25 mm GD/X syringe filter, Whatman$^®$, Maidstone, UK) and diluted with mobile phase in a 1:1 ratio. The exact concentration of TCR in each skin tested was quantified by using HPLC.

FT-IR imaging was performed to determine the distribution of TCR throughout the depth of the skin. After the ex vivo skin penetration test for 24 h, the skin was cut into 50 μm slices from top to bottom by using a cryomicrotome (Microm HM450, Thermo Scientific, Waltham, USA). Up to approximately 900 μm of the skin was obtained and cut vertically to determine the difference in TCR by depth. The skin slice was placed on a glass slide (Marinefield Superior, Lauda-Königshofen, Germany) and examined by FT-IR imaging (Cary 670 & Cary 620, Agilent$^®$ Technologies, Santa Clara, USA). In each experiment, the wavelength of 3450 cm^{-1} was used for analysis. Each IR field of view size was a square with sides of 352 μm and each IR pixel was a square with sides of 5.5 μm. In the FT-IR images, a red color indicated a relatively high concentration of TCR, whereas a blue color indicated a relatively low amount of TCR.

In vivo skin penetration of TCR-SLNs

The in vivo skin penetration test was performed by using a modified method described previously.[34] The hair on the dorsal skin of New Zealand white rabbits was shaved before the test compounds were applied to an 8×6 cm^2 area. The TCR-SLNs and reference product were each applied to five rabbits once daily for 2 weeks on the shaved skin. At 24 h after the last application, the rabbits were sacrificed. Any remaining drug on the area was removed with a cotton swab, and the skin was excised. A 50 μm slice was prepared using the same methods used for the FT-IR imaging. The residual amount of TCR in the horizontal section was analyzed by HPLC and FT-IR imaging.

Skin irritation in rabbits was evaluated by using the Draize test. The appearance of erythema was evaluated at 24 h after the final application. The dorsal skin was graded (Table 3) from no erythema (score: 0) to severe erythema (score: 4)[35] and the images of skin were scored by nine blinded observers.

Table 3 Grading scale for the Draize test

Grade	Formation of erythema
0	No erythema
1	Very slight erythema
2	Well-defined erythema
3	Moderate to severe erythema
4	Severe erythema

All animal experiments were conducted in accordance with the "Principles of Laboratory Animal Care" and approved by the Committee for Animal Experiments of Chungbuk National University (Cheongju, Korea).

Statistics

All statistical analyses were computed by using SPSS version 23 (SPSS Inc., IL, USA). Differences were determined using the Student's t-test with significance set at p-values of less than 0.05.

Results and discussion
Characterization of SLNs
Preparation of TCR-SLNs

Previous studies have shown that the elution pattern of SLNs was dependent on the lipids comprising the SLN.[36] Surfactants that form the shell of the particles were screened to obtain SLN with the desired thermosensitive properties. Poloxamer 188, PEG-40 stearate, Brij$^®$ 58, and PEG-1000 were chosen for the shell surfactant of thermosensitive SLNs (Table 1). The DSC profiles of the surfactant raw materials and SLN-Bs prepared with each surfactant are shown in Figure 1(A). The DSC profiles showed that the endothermic peak temperature of the prepared SLNs was generally relatively lower than that of the raw surfactant materials. The T_m of PEG-1000 was 31 °C and the T_m of SLN-B4 was 27 °C. This was too low for SLNs with PEG-1000 to remain stable at room temperature. The particles were relatively easily degraded and did not maintain their shape. For Brij$^®$ 58, which has a T_m of 38 °C, the T_m of SLN-B3 was 33 °C; this was the closest to body temperature. In contrast, the T_m of PEG-40 and Poloxamer 188 was approximately 50 °C and 60 °C, respectively; SLN-B1 and SLN-B2 displayed endothermic peaks at 48 °C and 46 °C. SLN-B1, which contained Poloxamer 188, had the highest T_m of the prepared blank-SLNs. Two candidate surfactants, Poloxamer 188 and Brij$^®$ 58, were selected, and SLNs made from these surfactants were examined for their physicochemical properties and subjected to in vitro/ex vivo testing. The final formulation that was chosen for further study is shown in Table 2. In the prepared TCR-SLN groups, the TCR content was 0.1% w/w, which was the same as that of reference product.

Physicochemical properties of TCR-SLNs

As shown in Table 4, the two prepared SLNs containing TCR had a mean particle size of 152.9±4.09 nm and 143.1 ±7.98 nm, respectively, and PDI values of 0.25±0.03 and
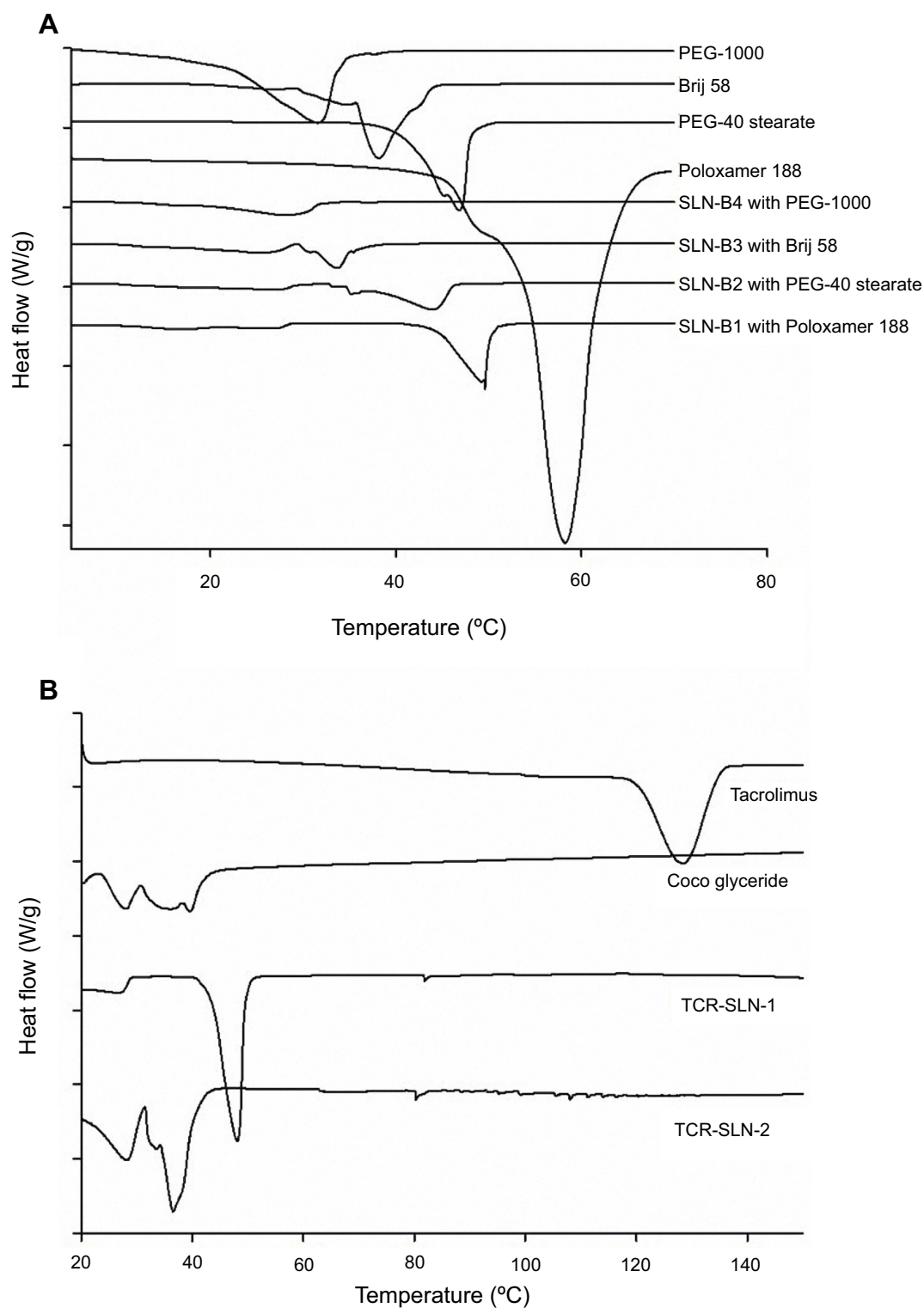
A

B

Figure I DSC thermograms of: (**A**) the raw surfactant and blank SLNs prepared with surfactant; (**B**) the raw materials and prepared TCR-SLNs.

0.27±0.02, respectively; despite the different surfactants, these values were not significantly different. These results showed that when the particles were manufactured in accordance with the indicated preparation method,[37]

small and uniform particles of approximately 150 nm were produced.

The drug entrapment efficiency is an important index to determine whether the prepared SLNs meet clinical

Table 4 Particle properties of TCR-SLNs (mean ± standard deviation)

	TCR-SLN-1	**TCR-SLN-2**
Mean particle size (nm)	152.9±4.09	143.1±7.98
Polydispersity index	0.25±0.03	0.27±0.02
Entrapment efficiency (%)	88.9±0.7	88.5±0.2

requirements and to judge their suitability as a drug carrier system. The term entrapment implies that the drug is positioned within the solid lipid matrix. As shown in Table 4, the entrapment efficient of TCR-SLN-1 and TCR-SLN-2 was 88.9% ±0.7% and 88.5% ±0.2%, respectively. The entrapment standard deviation was also low, indicating uniform entrapment. These results suggested that TCR is more abundant in the lipid phase (SLN) than in the aqueous phase, a result of the physicochemical properties of TCR such as high hydrophobicity, low solubility in water, and high log P.[38–40]

The DSC thermograms of raw TCR, cocoglyceride, and TCR-SLNs are shown in Figure 1(B). The breakdown of the crystalline lattice by heating, information about the lipid structure, and the possibility of polymorphisms, crystal ordering, or glass transition processes can be easily detected by DSC. The DSC thermogram of raw TCR showed one endothermic peak with an onset temperature at 128 °C, which was indicative of melting and the crystalline nature of the raw TCR; this also confirmed the XRD results. The thermogram of cocoglyceride showed a widened and split endothermic peak from 25 °C to 40 °C. The thermograms of prepared TCR-SLN-1 and TCR-SLN-2, made with Poloxamer 188 and Brij® 58 respectively, were most affected by the presence of surfactant. In addition, no TCR-SLNs exhibited characteristic TCR endothermic melting peaks, indicating that the TCR exists in an amorphous state within the TCR-SLNs. TCR-SLN-1 showed an endothermic peak at 48 °C, thought to be derived from Poloxamer 188, and an endothermic peak at approximately 28 °C from cocoglyceride. This was similar to B-SLN-1. TCR-SLN-2 showed endothermic peaks at 28 °C and 36 °C and endothermic peaks at higher temperatures than B-SLN-3 but formed at lower temperatures than the T_m of Brij® 58. Overall, an endothermic peak at approximately 28 °C, which is derived from cocoglyceride, was common in the TCR-SLNs. In addition, the main endothermic peak of TCR-SLNs shifted to a lower temperature compared with that of the raw surfactant. A reduction in the

T_m and enthalpy of the melting endotherm was observed when the lipid was formulated as TCR-SLNs.[41] Freitas and Muller also observed that the crystallization behavior of SLNs differed distinctly from that of the raw lipid.[42] The small particle size of SLNs results in a high surface energy, which creates an energetically suboptimal state that results in a decrease in the melting point.[43]

The XRD data shown in Figure 2 agreed well with the results from DSC. Powder XRD analysis offers the clear advantage of allowing the identification of the crystalline or amorphous state of lipid particles and their crystal modification. Raw TCR exhibited sharp and narrow diffraction peaks at 2θ of 5º–30º, which are characteristic of a high degree of long-range molecular order. Moreover, Poloxamer 188 and Brij® 58 showed two peaks at 2θ of 19º and 23º, and the two peaks of the surfactant contained in TCR-SLNs were weak. Furthermore, the diffraction pattern of the prepared TCR-SLNs differed considerably from that of raw TCR. The peaks of raw TCR mostly disappeared in the XRD pattern of TCR-SLNs, indicating that the crystal arrangement in the SLN formulations was less ordered than that in raw TCR. The loss of crystallinity in the XRD pattern of the lyophilized SLN was discerned through the absence of sharp peaks and the loss of most of the peaks of TCR.[44] Through comparison with earlier results, it was concluded that the drug entrapped in the prepared TCR-SLNs was in an amorphous or disordered crystalline phase of a molecular dispersion. The amorphous form is thought to have higher energy with a greater surface area and, subsequently, higher solubility, dissolution rates, and bioavailability.[45] These properties of the amorphous form are expected to facilitate overcoming
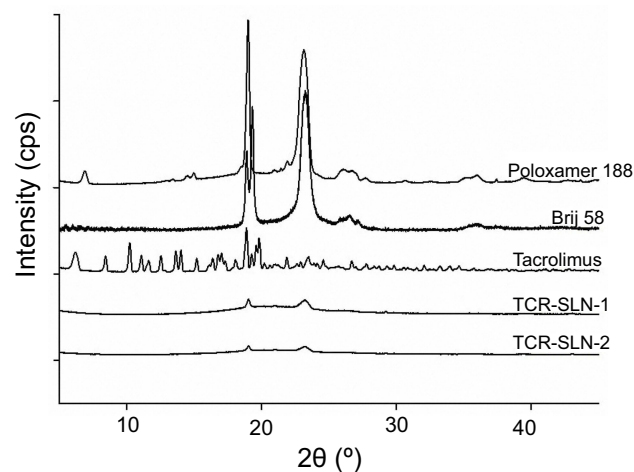
Figure 2 XRD patterns of the raw materials and prepared TCR-SLNs.

skin permeability barriers and conferring a significant improvement in bioavailability after absorption.

FT-IR analysis can provide further confirmation of the stability and crystallinity of prepared TCR-SLNs. In this study, raw TCR, Poloxamer 188, Brij[®] 58, prepared TCR-SLN-1 and −2, and physical mixtures of the TCR-SLN-1 and −2 composition were analyzed and the FT-IR spectra obtained were used as references for the evaluation of the lipid lattice structures of the prepared TCR-SLNs. The FT-IR spectra are shown in Figure 3. The spectrum of raw TCR was similar to previous studies that showed strong infrared absorption at 3446, 2935, and 1639 cm^{-1}.[7,46] These peaks correspond to O–H stretching, alkane C–H bonds, and the C=O bond of the carbonyl ester group.[47,48] The peaks of raw TCR were weak, but present in the physical mixture; however, the peaks of the prepared TCR-SLN-1 and −2 were shifted more and were wider than for the physical mixture. This result was likely attributable to the complete encapsulation of TCR, its interaction with the excipients, and the change in crystallinity.[49] These results agreed with the observations made by Lee et al during their study on encapsulation in SLNs.[50] As the peaks at 3450 cm^{-1} do not overlap peaks with other excipients and are more intense than the physical mixture, we used this as the wavelength for detection of FT-IR images and subsequent experiments (Figure 3).

TEM imaging can be used to directly identify the morphology of the prepared nanoparticles. The shape of the nanoparticles prepared with TCR is shown in Figure 4. The particles displayed round and homogenous shading, with a particle size of approximately 150 nm. This clearly supported the data for the particle size and polydispersity index values. The TCR-SLNs were surrounded by the hydrophilic Poloxamer aqueous solution owing to the previously described interfacial phenomenon.[51,52] The
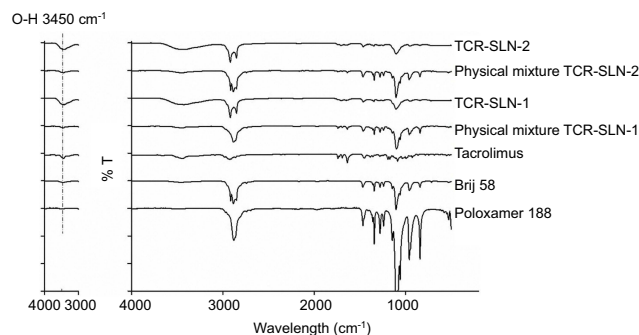
excellent stability is a result of the adequate surfactant content, including Poloxamer 188.[53,54] The TEM images obtained by drying at three different temperatures (25 °C, 37 °C, and 50 °C) are shown in Figure 4, and reveal the characteristics of the particles produced at different temperatures. For the TCR-SLN-1 particles dried at 37 °C (Figure 4(c)), the outer shape of the Poloxamer 188 maintained the structure well, but the particles became blurry and round and was slightly larger than that of particles dried at 25 °C. It appears that cocoglyceride changed from a solid to a liquid form, as indicated by the endothermic peak at approximately 28 °C in the DSC thermogram of TCR-SLNs. This is the reason for the extensibility of the molten SLNs.[55] Moreover, when the temperature of the particles was increased to 50 °C (Figure 4(e)), most did not maintain their shape and coagulated with other particles; alternatively, all the particles melted and did not maintain their shape. However, when TCR-SLN-2 was observed at these temperatures, a difference in particle shape was already visible at approximately 37 °C (Figure 4(D)). When dried at 37 °C, the shape of most of the particles was not maintained owing to the presence of Brij[®] 58 in TCR-SLN-2, and the size of the particles increased to a much greater extent than for TCR-SLN-1. After storage at 50 °C (Figure 4(F)), all particles had melted and merged, and the shape could not be determined. Therefore, through TEM imaging, it was confirmed that the surfactant played an important role in forming the shell to maintain the external shape of the particle; moreover, the properties of the internal solid lipid are also of significance to the maintenance of particle shape.

In vitro release test of TCR-SLNs

The in vitro drug release studies were performed by using modified Franz diffusion cells; in this study, modified Franz diffusion cells with a dialysis membrane with a pore size of 2.4 nm were used. The dialysis membrane retained the nanoparticles and allowed only the immediate transfer of the dissolved drug into the receiver compartment. The in vitro release test results for the prepared TCR-SLN-1 and TCR-SLN-2 formulations stored at three different temperatures are shown in Table 5. As the pore size of the membrane is 2.4 nm, it is sufficiently small compared with the particle size to ensure that only free drug can be transferred to the receptor phase. The percentage of TCR released from TCR-SLN-1 and TCR-SLN-2 after 24 h was 22.52% and 20.11%, respectively; there was no significant difference between these values. However, after storage at
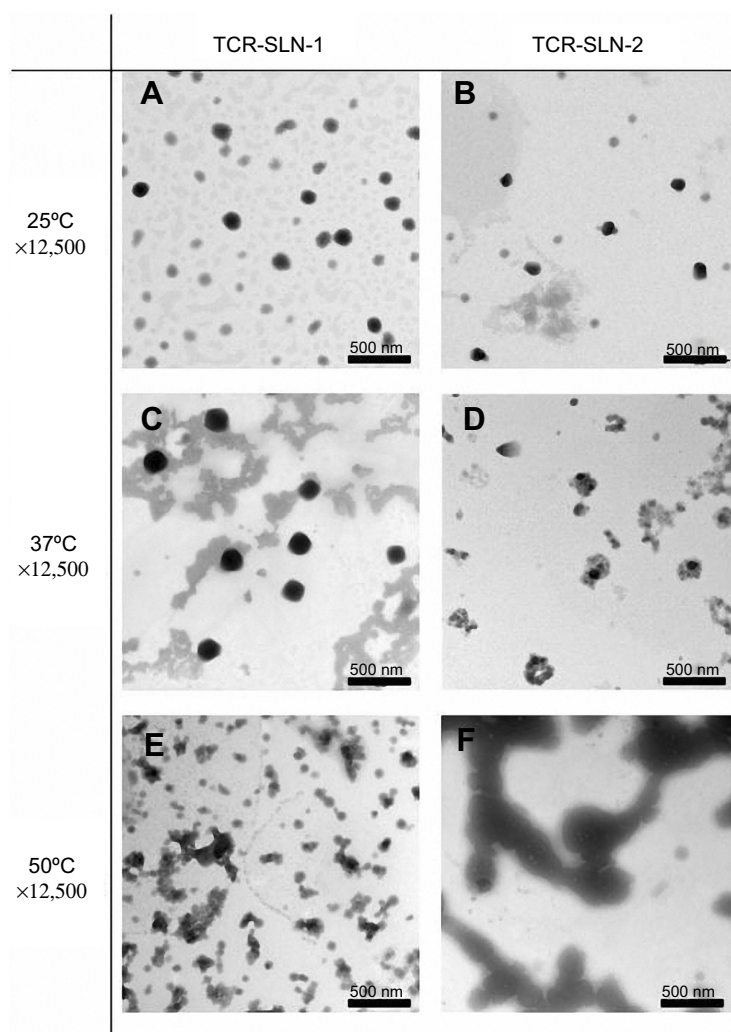

O-H 3450 cm^{-1}

%T

Wavelength (cm^{-1})

TCR-SLN-2
Physical mixture TCR-SLN-2
TCR-SLN-1
Physical mixture TCR-SLN-1
Tacrolimus
Brij 58
Poloxamer 188

Figure 3 FT-IR spectra of the raw materials, prepared TCR-SLNs, and physical mixtures of TCR-SLN materials.

Figure 4 TEM images of TCR-SLNs dried at different temperatures (magnification: ×12,500, scale bar =500 nm).

37 °C, TCR-SLN-2 displayed a significantly higher release than TCR-SLN-1, of approximately 37.80%, because the particles were almost completely fragmented and did not retain their shape, allowing the TCR dispersed in the lipid to pass through the membrane. In contrast, TCR-SLN-1 stored at 37 °C demonstrated approximately 28% release, which was higher than the release rate from TCR-SLN-1 stored at 25 °C, owing to lipid leakage, but constituted a smaller increase than that for TCR-SLN-2. The results correlated with the DSC and TEM results. In the TEM images after storage at 37 °C, TCR-SLN-2 appeared more melted than TCR-SLN-1. In addition, in the DSC thermogram, TCR-SLN-1 exhibited a main melting peak of above 37 °C, although there was a melting peak for cocoglyceride at approximately 28 °C. However, TCR-SLN-2 exhibited a main melting peak before 37 °C. The results of the in vitro test indicated that TCR-SLN-1 was more suitable for targeting the dermal layer: the outer skin temperature is 32 °C, but the dermal temperature is 37 °C; at this temperature, it is difficult for TCR-SLN-2 to maintain its shape. Furthermore, the amount released after storage of TCR-SLN-1 and TCR-SLN-2 at 50 °C was similar. High release percentages (48.55% and 46.96%) were obtained after treatment at 50 °C, because the morphology of the particles was not maintained and was completely destroyed, as shown in the TEM images. It was therefore confirmed that the state of the particles was dependent on temperature and greatly influenced the release rate. These thermodynamic differences are thought to have affected not only the morphology of the drug, but also the release rate. This also suggests the possibility of thermosensitive SLNs in which the particle maintains its morphology and penetrates as a nanoscale particle up to an outer skin temperature (32 °C), and then dissolves dermal temperature (37 °C).

Table 5 Amount of TCR accumulated in 24 h in the in vitro and ex vivo test conducted at 37 °C on TCR-SLNs stored at different temperatures for 2 h (mean ± standard error; *Student's *t*-test, *p*-value <0.05 with TCR-SLN-2; **Student's *t*-test, *p*-value <0.005 with TCR-SLN-2)

Storage temperature before test	Amount accumulated at 24 h after in vitro release test		Amount accumulated at 24 h after ex vivo skin deposition test	
	TCR-SLN-1	TCR-SLN-2	TCR-SLN-1	TCR-SLN-2
25 °C	22.52% ±1.17%	20.11% ±0.82%	21.82% ±4.38%	8.31% ±1.26%
37 °C	29.00% ±2.26%*	37.80% ±2.08%	16.89% ±1.45%**	3.80% ±0.58%
50 °C	48.55% ±0.30%	46.96% ±1.10%	14.16% ±1.84%**	4.57% ±0.21%

Ex vivo skin penetration test

To assess the skin penetration of TCR from the prepared TCR-SLNs, the ability to permeate the skin was assessed ex vivo by using a Franz diffusion cell. The amount of TCR remaining in the excised rat dorsal skin after 24 h of the permeation test is shown in Table 5. The concentration of TCR-SLN-1 was 2.6 times higher than that of than TCR-SLN-2 in the skin membrane, represented by the epidermis and dermis. This result indicated that although the external temperature of the Franz cells was 32 °C, TCR-SLN-2 had already melted on the membrane and accumulated on the skin with difficulty through the stratum corneum layer, owing to the degraded particles. In contrast, TCR-SLN-1, which was not melted, as seen in the TEM images, was able to penetrate the epidermis and dermis as intact nanoparticles. In addition, TCR was not detected in the receptor phase of either TCR-SLNs after the 24 h permeation test, suggesting that the particles remain in the skin layer and not diffuse into the receptor phase. These properties are expected to be effective for targeting drug delivery to the skin and reducing side effects from systemic circulation. The results of the same experiment using the samples stored 2 h at 37 °C and 50 °C are shown in Table 5. As the temperature increased, TCR-SLN-1 was unable to penetrate the skin, as the particles were already degraded; thus, the amount remaining on the membrane was relatively decreased. TCR-SLN-2 showed the same tendencies as TCR-SLN-1, but the difference was significant. For TCR-SLN-1 treatment at 50 °C, the residual amount in the skin layer decreased as expected. In summary, TCR-SLNs could penetrate the stratum corneum owing to the maintained morphology of the particles; and, after penetration into the dermis, the TCR-SLNs remained in the dermis without transition to the receptor phase owing to their high lipophilicity and release at dermal temperature. This demonstrated that thermosensitive SLNs were suitable for skin-targeted drug delivery. SLNs with a small diameter allowed the improved penetration of nanoparticles into the skin and the controlled release of SLNs induce an increase in drug accumulation.[56,57] In this study, permeation and penetration studies were also supported by previous analyses that focused on particle size. However, owing to the small particle size of our formulation, and the oil phase release temperature of the SLN, the amount remaining in a skin will increase. The slight difference between the average particle sizes of the TCR-SLNs formulations was not the key factor that influenced the drug penetration into the skin; it was the thermodynamic properties that resulted in release at a dermal temperature.

In this experiment, FT-IR imaging was used to confirm the depth of TCR penetration for each of the prepared TCR-SLNs and the reference product by using the skin used in the Franz-diffusion test. The FT-IR spectrum was monitored at 3450 cm^{-1} as a wavelength specific for TCR.[7] As shown in Figure 5, in the TCR-SLN-1, −2, and the reference product, a very large amount of TCR was detected in the stratum corneum. Overall, for all groups, TCR appeared to remain in the stratum corneum. The results of FT-IR imaging through the skin for the reference product confirmed that a specific wavelength for TCR appeared broadly in the stratum corneum, but was hardly present in the epidermis. In comparison, the FT-IR images of prepared TCR-SLN-1 and TCR-SLN-2 showed TCR in deeper layers, up to 450 μm depth, than the reference product. In addition, of the two TCR-SLNs, TCR-SLN-1 showed better permeability to deeper layers and a greater amount of penetrated TCR. Although a significant amount of TCR-SLN-1 penetrated up to 450 μm in depth, TCR-SLN-2 penetration was found to be very low, even at 300 μm. These results confirmed the ex vivo skin penetration test results. In the skin permeation test, TCR-SLN-1 resulted in not only the greatest amount penetrated, but also penetrated deeper into the skin layer. In addition, the failure to pass through the receptor phase was a
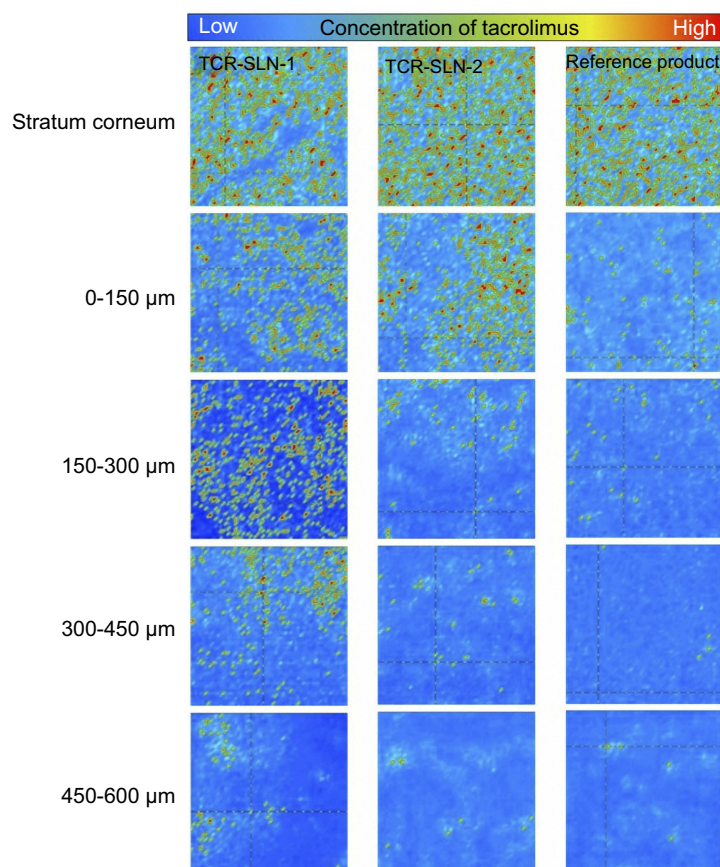
Figure 5 FT-IR imaging of the stratum corneum and skin at different depths after ex vivo skin penetration test at 37 °C using the reference product and TCR-SLNs.

result of the formulation release at a dermal temperature, preventing penetration into the deeper layers of skin.
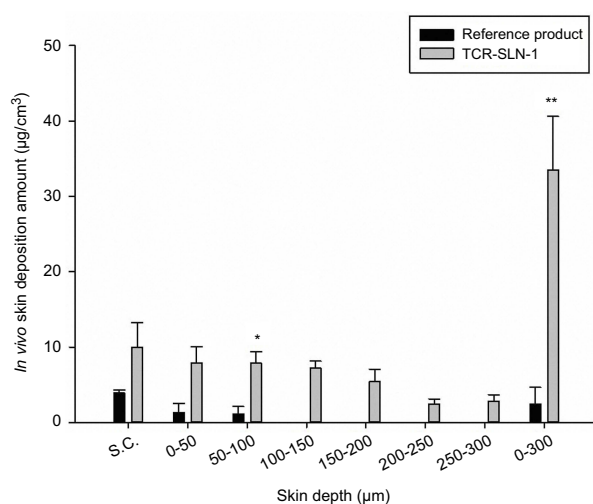

Figure 6 In vivo skin penetration test using reference product and TCR-SLN-1 (mean ± standard error; S.C.: stratum corneum, *Student's t-test, p-value <0.05 compared with the reference product; **Student's t-test, p-value <0.01 compared with the reference product).

In vivo evaluation of TCR-SLNs
In vivo skin penetration test of TCR-SLNs

The residual amount of TCR in the skin, as determined by HPLC analysis of rabbit skin treated with TCR-SLN-1 and reference product once daily for 2 weeks, is shown in Figure 6. Overall, as observed in the ex vivo study, TCR-SLN-1 delivered more drug to deeper skin layers than the reference product. TCR-SLN-1 permeated from the stratum corneum to 300 μm depth, and reference product was not detected from 150 μm depth. The results were statistically significant at depths of 50–100 μm, 100–150 μm, and 0–300 μm. A large amount of TCR was detected at depths of 0–300 μm, indicating that TCR-SLN-1 had penetrated deeper dermis layers. In addition, in the in vivo test results, penetration was greater than in the ex vivo tests. The drug appeared to accumulate after administration for 2 weeks. Plasma concentration was not measured, but it is expected that almost no migration to blood will occur, as shown by the ex vivo test.

The FT-IR imaging of TCR throughout the skin depth in the in vivo skin penetration study is shown in Figure 7. Similar to the ex vivo results, the highest intensities of
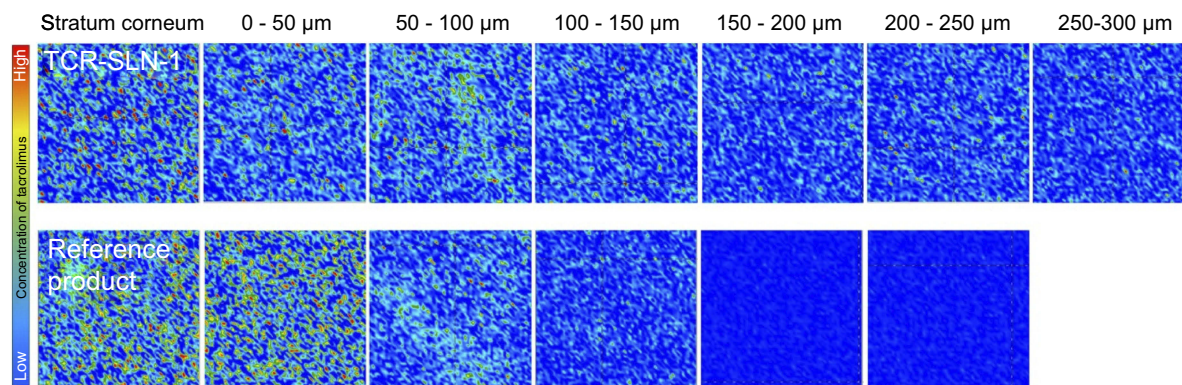
Figure 7 FT-IR imaging of the stratum corneum and skin at different depths after in vivo skin penetration test using the reference product and TCR-SLN-1.

TCR were found in the stratum corneum after administration of both the reference product and TCR-SLN-1, and gradually decreased as the skin deepened. For the reference product, TCR was not detectable below 150 µm. In contrast, TCR-SLN-1 was present in large quantities up to 300 µm and was detected faintly at 500 µm (data not shown). These results were highly correlated with the results in Figure 6 and FT-IR is considered to be able to detect even small amounts of TCR in deeper skin layers, as it directly detects TCR without the requirement for processes such as extraction or dilution. The results of the in vivo permeation test by skin depth using HPLC and FT-IR imaging were very similar, as were the ex vivo results. In addition, it was confirmed that TCR-SLN-1 penetrated into the deep skin layers owing to its small size. The in vitro test results suggest that drug release would occur from the formulation remaining in the skin layer after penetration.

Skin irritation test

Skin irritation was assessed by the appearance of erythema and was assessed at 24 h after the final application. Five animals were assigned to each group, and nine were scored with a pre-classified score of 0–4 (Table 3) from a blinded assessment of images of the skin. The score after reference product treatment was 2.7, which suggested that the induced erythema was significantly more severe than that induced by TCR-SLN-1 (Score 1.2, Table 6). In Table 1,

the image of each group before and after drug administration is shown. In each group, the rabbits that received the highest score and the lowest score for rabbit skin are presented. The skin treated with reference product displayed severe erythema; it is thought that the irritation occurs owing to the various excipients in the ointment.[58,59] In contrast, the images after TCR-SLN-1 application to rabbit skin yielded no irritation. Even the skin with the highest score among the TCR-SLN-1 groups only displayed weak reddening.

Conclusion

These experimental results showed that TCR, a drug that cannot easily penetrate through the skin and has properties unsuitable for transdermal use, could be encapsulated in thermosensitive SLNs to produce relatively stable particles that accumulated in skin. It was confirmed that the surfactant in the shell of the particles affected the release properties. In general, the breaking point, at which a particle loses its shape, was dependent on the temperature of the surfactant: the lower the melting point of the surfactant, the greater the extent of degradation at low temperatures, even below room temperature. Among surfactants, two candidates were selected and their physicochemical properties were determined. The entrapment efficiency was 88%, which showed that more TCR was present in the SLN than in the aqueous phase. In addition, DSC, XRD, and FT-IR spectra showed that TCR was dispersed in the lipid inside the surfactant shell in an amorphous form. Finally, TEM was used to determine the morphology of prepared SLNs and the images were compared with DSC data to confirm that the appearance under different conditions was dependent on the temperature. Characterization of the TCR-SLNs was performed by using an in vitro release test, an ex vivo skin penetration test, and FT-IR imaging. Two candidate formulations, TCR-SLN-1 and TCR-SLN-2, were produced

Table 6 Skin irritation test of the reference product and TCR-SLN-1 (mean ± standard error; **Student's t-test, p-value <0.005 compared with the reference product)

	TCR-SLN-1	**Reference product**
Score	1.24±0.14**	2.71±0.07

and the release and skin penetration tests were performed for each candidate group at different temperatures. The release test showed significant differences in the prepared SLNs treated at 37 °C. This suggested that thermosensitive SLNs that released at a dermal temperature have been successfully manufactured. In addition, the skin penetration test showed a significant difference according to the treatment temperature of the sample, with a difference in the skin accumulation amount. These results suggested that thermosensitive SLNs prepared by using the thermodynamic properties that are dictated by the surfactant will provide enhanced drug delivery to the skin. An in vivo comparison of TCR-SLN-1 and the reference product was performed. The degree of skin penetration of TCR was evaluated by HPLC and FT-IR imaging methods. These two methods showed very similar results. Furthermore, similar to the ex vivo tests, TCR-SLN-1 permeated into a deeper layer.

In conclusion, thermosensitive SLNs with different thermodynamic properties, dictated by the type of surfactant forming the shell, are very effective for topical drug delivery. This effect was confirmed in ex vivo and in vivo tests and was visualized by using FT-IR imaging.

Acknowledgments

Disclosure

The authors declare that they have no conflicts of interest in this work.

References

1. Chang K-T, Lin -HY-H, Kuo C-H, Hung C-H. Tacrolimus suppresses atopic dermatitis-associated cytokines and chemokines in monocytes. *J Microbiol Immunol Infect*. 2016;49:409–416. doi:10.1016/j.jmii.2014.07.006

2. Zhang D, Pan X, Wang S, et al. Multifunctional poly (methyl vinyl ether-co-maleic anhydride)-graft-hydroxypropyl-β-cyclodextrin amphiphilic copolymer as an oral high-performance delivery carrier of tacrolimus. *Mol Pharm*. 2015;12:2337–2351. doi:10.1021/acs.molpharmaceut.5b00010

3. Goebel AS, Neubert RH, Wohlrab J. Dermal targeting of tacrolimus using colloidal carrier systems. *Int J Pharm*. 2011;404:159–168. doi:10.1016/j.ijpharm.2010.11.029

4. Lei W, Yu C, Lin H, Zhou X. Development of tacrolimus-loaded transfersomes for deeper skin penetration enhancement and therapeutic effect improvement in vivo. *Asian J Pharma Sci*. 2013;8:336–345. doi:10.1016/j.ajps.2013.09.005

5. Lapteva M, Mondon K, Möller M, Gurny R, Kalia YN. Polymeric micelle nanocarriers for the cutaneous delivery of tacrolimus: a targeted approach for the treatment of psoriasis. *Mol Pharm*. 2014;11:2989–3001. doi:10.1021/mp400639e

6. Shin S-B, Cho H-Y, Kim D-D, Choi H-G, Lee Y-B. Preparation and evaluation of tacrolimus-loaded nanoparticles for lymphatic delivery. *Eur J Pharm Biopharm*. 2010;74:164–171. doi:10.1016/j.ejpb.2009.08.006

7. Pople PV, Singh KK. Development and evaluation of colloidal modified nanolipid carrier: application to topical delivery of tacrolimus. *Eur J Pharm Biopharm*. 2011;79:82–94. doi:10.1016/j.ejpb.2011.02.016

8. Desfrançois C, Auzély R, Texier I. Lipid nanoparticles and their hydrogel composites for drug delivery: A review. *Pharmaceuticals*. 2018;11:118–145. doi:10.3390/ph11040118

9. Aljaeid BM, Hosny KM. Miconazole-loaded solid lipid nanoparticles: formulation and evaluation of a novel formula with high bioavailability and antifungal activity. *Int J Nanomedicine*. 2016;11:441–447. doi:10.2147/IJN.S100625

10. Liu B, Han L, Liu J, Han S, Chen Z, Jiang L. Co-delivery of paclitaxel and TOS-cisplatin via TAT-targeted solid lipid nanoparticles with synergistic antitumor activity against cervical cancer. *Int J Nanomedicine*. 2017;12:955–968. doi:10.2147/IJN.S115136

11. Kumar R, Singh A, Garg N, Siril PF. Solid lipid nanoparticles for the controlled delivery of poorly water soluble non-steroidal anti-inflammatory drugs. *Ultrason Sonochem*. 2018;40:686–696. doi:10.1016/j.ultsonch.2017.08.018

12. Rupenagunta A, Somasundaram I, Ravichandiram V, Kausalya J, Senthilnathan B. Solid lipid nanoparticles-A versatile carrier system. *J Pharma Res*. 2011;4:2069–2075.

13. Zoubari G, Staufenbiel S, Volz P, Alexiev U, Bodmeier R. Effect of drug solubility and lipid carrier on drug release from lipid nanoparticles for dermal delivery. *Eur J Pharm Biopharm*. 2017;110:39–46. doi:10.1016/j.ejpb.2016.10.021

14. Ud Din F, Aman W, Ullah I, et al. Effective use of nanocarriers as drug delivery systems for the treatment of selected tumors. *Int J Nanomedicine*. 2017;12:7291–7309. doi:10.2147/IJN.S146315

15. Choi YH, Han H-K. Nanomedicines: current status and future perspectives in aspect of drug delivery and pharmacokinetics. *J Pharm Investig*. 2018;48:43–60. doi:10.1007/s40005-017-0370-4

16. Saporito F, Sandri G, Bonferoni MC, et al. Essential oil-loaded lipid nanoparticles for wound healing. *Int J Nanomedicine*. 2018;13:175–186. doi:10.2147/IJN.S152529

17. Lohan SB, Bauersachs S, Ahlberg S, et al. Ultra-small lipid nanoparticles promote the penetration of coenzyme Q10 in skin cells and counteract oxidative stress. *Eur J Pharm Biopharm*. 2015;89:201–207. doi:10.1016/j.ejpb.2014.12.008

18. Oliveira MS, Mussi SV, Gomes DA, et al. α-Tocopherol succinate improves encapsulation and anticancer activity of doxorubicin loaded in solid lipid nanoparticles. *Colloid Surf B Biointerfaces*. 2016;140:246–253. doi:10.1016/j.colsurfb.2015.12.019

19. Ding Y, Pyo S, Müller R. smartLipids® as third solid lipid nanoparticle generation–stabilization of retinol for dermal application. *Die Pharmazie Int J Pharma Sci*. 2017;72:728–735.

20. Schäfer-Korting M, Mehnert W, Korting H-C. Lipid nanoparticles for improved topical application of drugs for skin diseases. *Adv Drug Deliv Rev*. 2007;59:427–443. doi:10.1016/j.addr.2007.04.006

21. Dabbagh A, Abdullah BJJ, Abu Kasim NH, Abdullah H, Hamdi M. A new mechanism of thermal sensitivity for rapid drug release and low systemic toxicity in hyperthermia and thermal ablation temperature ranges. *Int J Hyperthermia*. 2015;31:375–385. doi:10.3109/02656736.2015.1006268

22. Cha JM, You DG, Choi EJ, et al. Improvement of antitumor efficacy by combination of thermosensitive liposome with high-intensity focused ultrasound. *J Biomed Nanotechnol*. 2016;12:1724–1733. doi:10.1166/jbn.2016.2272

23. Sarwal A, Singh G, Singh S, Singh K, Sinha V. Novel and effectual delivery of an antifungal agent for the treatment of persistent vulvo-vaginal candidiasis. *J Pharm Investig*. 2019;49:135–147. doi:10.1007/s40005-018-0395-3

24. Centelles MN, Wright M, So P-W, et al. Image-guided thermosensitive liposomes for focused ultrasound drug delivery: using NIRF-labelled lipids and topotecan to visualise the effects of hyperthermia in tumours. *J Control Release*. 2018;280:87–98. doi:10.1016/j.jconrel.2018.04.047

25. Guo Y, Zhang Y, Ma J, et al. Light/magnetic hyperthermia triggered drug released from multi-functional thermo-sensitive magnetolipo-somes for precise cancer synergetic theranostics. *J Control Release*. 2018;272:145–158. doi:10.1016/j.jconrel.2017.04.028

26. Park SM, Kim MS, Park S-J, et al. Novel temperature-triggered lipo-some with high stability: formulation, in vitro evaluation, and in vivo study combined with high-intensity focused ultrasound (HIFU). *J Control Release*. 2013;170:373–379. doi:10.1016/j.jconrel.2013.06.003

27. Kim YT, Ma D, Sim JK, Kim S-H. Simultaneous evaluation of thermal and non-thermal effects of high-intensity focused ultrasound on a tissue-mimicking phantom. *Ultrasound Med Biol*. 2018;44:1799–1809. doi:10.1016/j.ultrasmedbio.2018.03.024

28. Tagami T, Foltz WD, Ernsting MJ, et al. MRI monitoring of intratu-moral drug delivery and prediction of the therapeutic effect with a multifunctional thermosensitive liposome. *Biomaterials*. 2011;32:6570–6578. doi:10.1016/j.biomaterials.2011.05.029

29. Kim HR, You DG, Park S-J, et al. MRI monitoring of tumor-selective anticancer drug delivery with stable thermosensitive liposomes trig-gered by high-intensity focused ultrasound. *Mol Pharm*. 2016;13:1528–1539. doi:10.1021/acs.molpharmaceut.6b00013

30. Maniyar MG, Kokare CR. Formulation and evaluation of spray dried liposomes of lopinavir for topical application. *J Pharm Investig*. 2019;49:259–270. doi:10.1007/s40005-018-0403-7

31. Im GJ, Chae SY, Lee KC, Lee DS. Controlled release of insulin from pH/temperature-sensitive injectable pentablock copolymer hydrogel. *Journal of Controlled Release*. 2009;137:20–24. doi:10.1016/j.jconrel.2009.02.021

32. Trotta M, Debernardi F, Caputo O. Preparation of solid lipid nano-particles by a solvent emulsification–diffusion technique. *Int J Pharm*. 2003;257:153–160.

33. Praça FSG, Medina WSG, Eloy JO, et al. Evaluation of critical parameters for in vitro skin permeation and penetration studies using animal skin models. *Eur J Pharm Sci*. 2018;111:121–132. doi:10.1016/j.ejps.2017.09.034

34. Rubins A, Gutmane R, Valdmane N, Stevenson P, Foster C, Undre N. Pharmacokinetics of 0.1% tacrolimus ointment after first and repeated application to adults with moderate to severe atopic dermatitis. *J Invest Dermatol*. 2005;125:68–71. doi:10.1111/j.0022-202X.2005.23754.x

35. Park C-W, Kim J-Y, Rhee Y-S, et al. Preparation and valuation of a topical solution containing eutectic mixture of itraconazole and phenol. *Arch Pharm Res*. 2012;35:1935–1943. doi:10.1007/s12272-012-1110-y

36. Xie S, Zhu L, Dong Z, et al. Preparation, characterization and pharmacokinetics of enrofloxacin-loaded solid lipid nanoparticles: influences of fatty acids. *Colloid Surf B Biointerfaces*. 2011;83:382–387. doi:10.1016/j.colsurfb.2010.12.014

37. Wang R, Li L, Wang B, Zhang T, Sun L. FK506-loaded solid lipid nanoparticles: preparation, characterization and in vitro transdermal drug delivery. *Afr J Pharm Pharmacol*. 2012;6:904–913.

38. Kalepu S, Nekkanti V. Insoluble drug delivery strategies: review of recent advances and business prospects. *Acta Pharm Sin B*. 2015;5:442–453. doi:10.1016/j.apsb.2015.07.003

39. Pople PV, Singh KK. Targeting tacrolimus to deeper layers of skin with improved safety for treatment of atopic dermatitis. *Int J Pharm*. 2010;398:165–178. doi:10.1016/j.ijpharm.2010.07.008

40. Jain S, Addan R, Kushwah V, Harde H, Mahajan RR. Comparative assessment of efficacy and safety potential of multifarious lipid based Tacrolimus loaded nanoformulations. *Int J Pharm*. 2019;562:96–104. doi:10.1016/j.ijpharm.2019.03.042

41. Kim K-T, Lee HS, Lee J-J, et al. Nanodelivery systems for over-coming limited transportation of therapeutic molecules through the blood–brain barrier. *Future Med Chem*. 2018;10:2659–2674. doi:10.4155/fmc-2018-0208

42. Freitas C, Müller R. Correlation between long-term stability of solid lipid nanoparticles (SLN™) and crystallinity of the lipid phase. *Eur J Pharm Biopharm*. 1999;47:125–132.

43. Jawahar N, Baruah UK, Singh V. Co-delivery of chloroquine phosphate and azithromycin nanoparticles to overcome drug resistance in malaria through intracellular targeting. *J Pharma Sci Res*. 2019;11:33–40.

44. Pathak P, Nagarsenker M. Formulation and evaluation of lidocaine lipid nanosystems for dermal delivery. *AAPS PharmSciTech*. 2009;10:985–992. doi:10.1208/s12249-009-9287-1

45. Corrigan DO, Healy AM, Corrigan OI. The effect of spray drying solutions of bendroflumethiazide/polyethylene glycol on the physico-chemical properties of the resultant materials. *Int J Pharm*. 2003;262:125–137.

46. Oh D-W, Kang J-H, Lee H-J, et al. Formulation and in vitro/in vivo evaluation of chitosan-based film forming gel containing ketoprofen. *Drug Deliv*. 2017;24:1056–1066. doi:10.1080/10717544.2017.1346001

47. Lee H-J, Kang J-H, Lee H-G, et al. Preparation and physicochemical characterization of spray-dried and jet-milled microparticles contain-ing bosentan hydrate for dry powder inhalation aerosols. *Drug Des Devel Ther*. 2016;10:4017–4030. doi:10.2147/DDDT.S120356

48. Pople PV, Singh KK. Development and evaluation of colloidal mod-ified nanolipid carrier: application to topical delivery of tacrolimus, Part II–in vivo assessment, drug targeting, efficacy, and safety in treatment for atopic dermatitis. *Eur J Pharm Biopharm*. 2013;84:72–83. doi:10.1016/j.ejpb.2012.11.026

49. Park C-W, Lee H-J, Oh D-W, Kang J-H, Han C-S, Kim D-W. Preparation and in vitro/in vivo evaluation of PLGA microspheres containing norquetiapine for long-acting injection. *Drug Des Devel Ther*. 2018;12:711–719. doi:10.2147/DDDT.S151437

50. Lee G-S, Lee D-H, Kang K-C, Lee C-I, Pyo H-B, Choi T-B. Preparation and characterization of bis-ethylhexyloxyphenolmethox-yphenyltriazine (BEMT) loaded solid lipid nano-particles (SLN). *J Ind Eng Chem*. 2007;13:1180–1187.

51. Din F, Choi JY, Kim DW, et al. Irinotecan-encapsulated double-reverse thermosensitive nanocarrier system for rectal administration. *Drug Deliv*. 2017;24:502–510. doi:10.1080/10717544.2016.1272651

52. Park JH, Kim DS, Mustapha O, et al. Comparison of a revaprazan-loaded solid dispersion, solid SNEDDS and inclusion compound: physicochemical characterisation and pharmacokinetics. *Colloid Surf B Biointerfaces*. 2018;162:420–426. doi:10.1016/j.colsurfb.2017.12.017

53. Ud Din F, Mustapha O, Kim DW, et al. Novel dual-reverse thermo-sensitive solid lipid nanoparticle-loaded hydrogel for rectal adminis-tration of flurbiprofen with improved bioavailability and reduced initial burst effect. *Eur J Pharm Biopharm*. 2015;94:64–72. doi:10.1016/j.ejpb.2015.04.019

54. Jeong SC, Kim DS, Jin SG, et al. Development of a novel celecoxib-loaded nanosuspension using a wet media milling process. *Die Pharmazie Int J Pharma Sci*. 2018;73:498–502.

55. Urbán-Morlán Z, Ganem-Rondero A, Melgoza-Contreras LM, Escobar-Chávez JJ, Nava-Arzaluz MG, Quintanar-Guerrero D. Preparation and characterization of solid lipid nanoparticles contain-ing cyclosporine by the emulsification-diffusion method. *Int J Nanomedicine*. 2010;5:611–620. doi:10.2147/IJN.S12125

56. Garcês A, Amaral M, Lobo JS, Silva A. Formulations based on solid lipid nanoparticles (SLN) and nanostructured lipid carriers (NLC) for cutaneous use: A review. *Eur J Pharm Sci*. 2018;112:159–167. doi:10.1016/j.ejps.2017.11.023

57. El-Housiny S, Shams Eldeen MA, El-Attar YA, et al. Fluconazole-loaded solid lipid nanoparticles topical gel for treatment of pityriasis versicolor: formulation and clinical study. *Drug Deliv*. 2018;25:78–90. doi:10.1080/10717544.2017.1413444

58. Hansen L, Lange R, Gupta S. Development and evaluation of a guideline for monitoring propylene glycol toxicity in pediatric intensive care unit patients receiving continuous infusion lorazepam. *J Pediatr Pharmacol Ther.* 2015;20:367–372. doi:10.5863/1551-6776-20.5.367

59. Petry T, Bury D, Fautz R, et al. Review of data on the dermal penetration of mineral oils and waxes used in cosmetic applications. *Toxicol Lett.* 2017;280:70–78. doi:10.1016/j.toxlet.2017.07.899
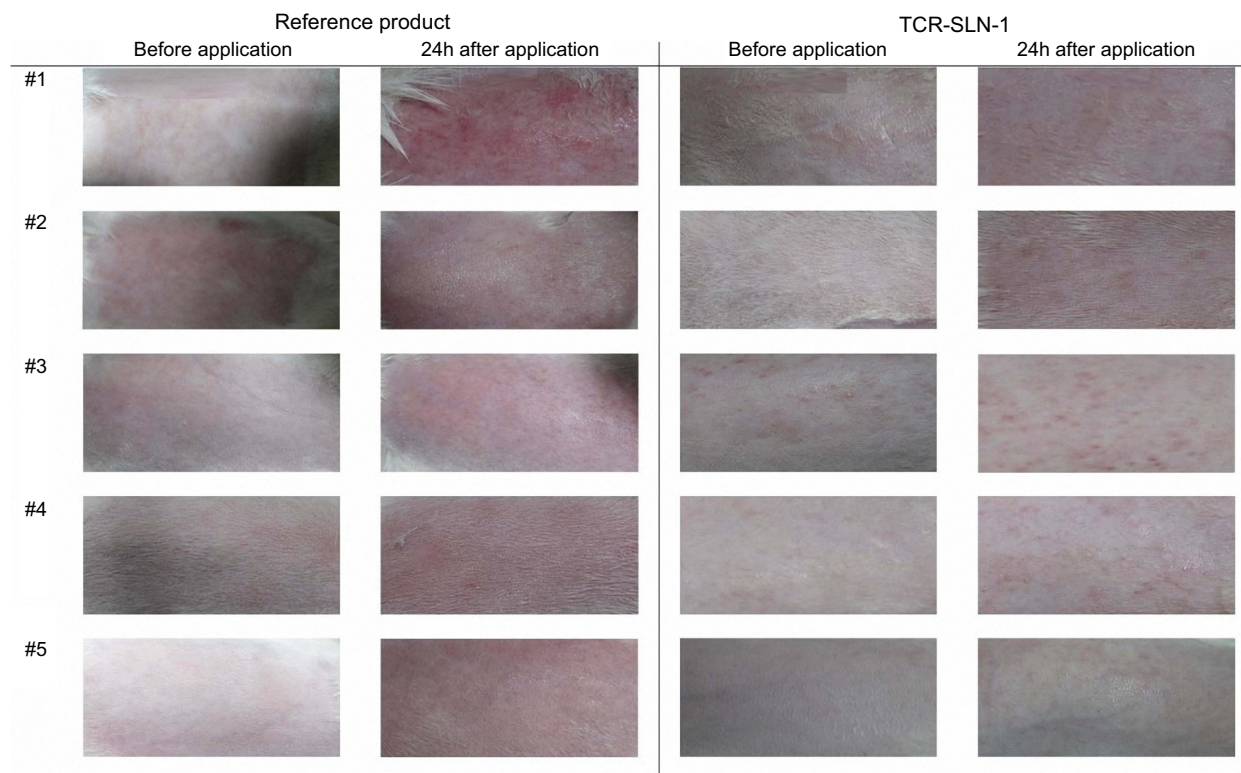
Supplementary materials

Figure S1 Images of skin samples from each group (24h after drug application).